Electrical Power and Energy Systems 125 (2021) 106468

Contents lists available at ScienceDirect

Electrical Power and Energy Systems

journal homepage: www.elsevier.com/locate/ijepes

Robust decentralized voltage control for uncertain DC microgrids

Marjan Shafiee-Rad[a], Mahdieh S. Sadabadi[b], Qobad Shafiee[c], Mohammad Reza Jahed-Motlagh[a,*]

[a] Department of Electrical Engineering, Iran University of Science and Technology, Tehran, Iran
[b] Department of Automatic Control and Systems Engineering, University of Sheffield, Sheffield, United Kingdom
[c] Smart/Micro Grids Research Center, Department of Electrical Engineering, University of Kurdistan, Sanandaj, Kurdistan, Iran

ARTICLE INFO

Keywords:
DC microgrids
Decentralized control
Linear matrix inequality (LMI)
Polytopic system
Robust performance
Robust stability

ABSTRACT

A decentralized voltage control scheme to achieve robust stability and robust performance of islanded direct current (DC) microgrids is presented in this paper. The investigated microgrid consists of multiple distributed generation (DG) units with a general topology, each one comprising a local uncertain ZIP (constant impedance (Z), constant current (I), and constant power (P)) load. The proposed controller confers the following main advantages: 1) the design procedure is scalable, 2) it has a completely decentralized structure, 3) it prepares stability and desirable performance of the nominal closed-loop microgrid, 4) it preserves robust stability as well as robust performance of microgrid system under different sources of uncertainty, including plug-and-play (PnP) functionalities of DGs, microgrid topology changes, uncertain ZIP load, and unmodeled load dynamics, 5) every local controller is the solution of a unique convex optimization problem, resulting in the optimal performance and robustness to several different successive changes. First, a linear time-invariant (LTI) state-space model is developed for each DG subsystem with capturing disturbances, and different uncertainty sources are modeled as a new single polytope. Then, all control objectives are converted into a robust dynamic output-feedback-based controller for an LTI polytopic system with $\boldsymbol{H}_\infty$ performance criterion. Finally, the obtained nonconvex problem is reduced to a linear matrix inequality (LMI) based optimization problem. Several simulation case studies are carried out in MATLAB to demonstrate the effectiveness of the proposed controller.

1. Introduction

In the last few decades, the increasing utilization of electrical energy, the restriction of fossil fuel sources, and their adverse environmental effects have led to a propensity towards distributed generations that contain renewable energy sources (RES), energy storage systems (ESS), and different types of loads. The integrated and reliable junction of DG units to the main power network was gained through microgrids [1].

Microgrids can operate in autonomous (islanded) or grid-connected mode, and based on the voltage type at the point of common coupling (PCC), AC and DC microgrids can be discerned [2]. While considerable development has been made to improve the performance of AC microgrids within the past years, for different uses DC microgrids have received more attention due to, 1) their higher efficiency, 2) more natural interface to many types of RES and ESS, 3) not requiring the control of the frequency, power quality, and reactive power, resulting in a remarkably less intricate control system, and 4) vast application in electrical vehicles, aircrafts, submarines, naval ships, telecom systems, etc. [3,4].

The connection of DGs to a DC microgrid is maintained via a controllable power electronic converter, and the main control objective is the adjustment of the voltage of the DC bus. In grid-connected mode, the main network imposes the voltage of the PCC. In contrast, in islanded mode, the microgrid needs a different control mechanism to regulate the load voltage of each DG unit and maintain the stability of the system. Droop control is a prevalent method to attain this utilizing decentralized proportional voltage control of several converters without digital communication links [4–9]. This approach is based on augmentation of a so-called virtual resistance (VR) control loop on top of the converter's voltage regulator, which permits current sharing and PnP functionalities at the same time [7]. However, in spite of these remarkable properties, several disadvantages restrict the usability of the droop controller, the most important ones being, load-dependent voltage deviation, steady-state error in voltage magnitudes, and the reality that diffusion of voltage error along resistive connection lines leads to current sharing deterioration [2]. To restore the voltage, a secondary controller, and to provide precise current sharing between different buses, a tertiary controller need to be applied [1–3]. Other disadvantages of the conventional droop method are its inability to

* Corresponding author at: Department of Electrical Engineering, Iran University of Science and Technology, Tehran 16846-13114, Iran.
E-mail address: jahedmr@iust.ac.ir (M.R. Jahed-Motlagh).

https://doi.org/10.1016/j.ijepes.2020.106468
Received 1 May 2020; Received in revised form 19 July 2020; Accepted 21 August 2020

attain a coordinated performance of multiple components with various characteristics, the compromise between power-sharing accuracy and voltage regulation, weak performance in the presence of resistive-inductive lines and/or conductance, and slow transient response [5].

Recently, to resolve some of the drawbacks related to the droop-based methods, non-droop-based control approaches have been presented in the literature [10–25]. In these methods, an advanced model-based controller performs the tasks of the primary and secondary controller related to the droop mechanism based on the received set points from the supervisory level. Controller design based on the robust stability and robust desirable performance approach under various sources of uncertainty, such as uncertain and unknown dynamics loads, PnP functionality of DGs, and changes in microgrid topology, has played a significant role among non-droop-based control manners. Robust stability means that the closed-loop system under the designed controller is stable in presence of uncertainties in the plant. As a result, the output will be bounded for every bounded input to the system and any finite initial condition. Besides, robust performance is defined as the closed-loop system's desirable performance, such as reference tracking with zero steady-state error, bounded control signal, acceptable transient response, etc., is always provided under existing uncertainty sources [26]. These strategies consider the robust voltage regulation of the autonomous microgrids to design a multi-loop state-feedback [12,13,19,20,22–24] or a single-loop output-feedback controller [10,11,14,15,18]. Due to their requirement for more measurement sensors and also the availability or estimation of all state variables, state-feedback-based methods impose higher costs and lower system reliability. As a result, these control manners are less appropriate for actual implementation.

Robust non-droop-based methods have been mostly used to control the voltage of AC islanded microgrids [10–16]. Several control schemes have recently been presented for DC autonomous microgrids [17–25]. A Non-fragile robust H_∞ approach is proposed in [17] to minimize the effects of the modelling uncertainty and the external disturbance in DC microgrids with parallel topology. A centralized output-feedback controller is proposed in [18] that only guarantees robustness against unknown loads and parametric uncertainties of the DGs. Another centralized controller based on state-feedback is designed in [19] with robustness against load changes and parametric uncertainties. A decentralized nonlinear state-feedback based controller is presented in [20], which is robust with respect to bounded unknown disturbances. However, the load dynamics are neglected in [18–20]. A nonlinear decentralized backstepping-based strategy is proposed in [21] to improve the transient response in the presence of load change and constant power load (CPL). A decentralized state-feedback controller is suggested in [22] that guarantees robust stability against uncertain CPL, and uncertain constant impedance load (CIL). To resolve the problem of voltage regulation of the DC microgrid in case of PnP functionality of DGs, the state-feedback control approaches have been used in [23,24]. These are based on the neutral interactions idea and have a decentralized scalable structure. In the provided control method in [23], after plugging in/out of a DG unit, all the local controllers of its neighboring DGs needed redesigning, which resulted in the complexity of the proposed controller. A three degree-of-freedom (DOF) control scheme is propounded in [24], with no need to retune the state-feedback gains after the PnP operations of DG units. Nevertheless, the developed strategies in [23,24] do not take into account load dynamics. Also, these approaches use static state-feedback to provide system stability and two pre-filters to reduce the load effect and improve the dynamic output of the closed-loop microgrid. Although the introduced state-feedback-based controllers satisfy robust stability, robust desirable performance of the system is not guaranteed. Moreover, the design of the pre-filters and state-feedback gains are accomplished as three independent optimization problems, which leads to a suboptimal controller, and as a results the suboptimal closed-loop performance and non-robustness to several subsequent changes caused by different sources of uncertainty. Furthermore, using the neutral interactions idea results in some restrictions to the decision variables in the final optimization problem, which leads to a more conservative control design approach. Various researches have been conducted on the extension of robust non-droop-based control for DC microgrids; however, they comprise one or more of the following disadvantages, 1) non-robustness with respect to PnP functionality of DGs [18–20], 2) non-robustness against uncertain ZIP loads [18–21,23,24], 3) inability to maintain robust performance under PnP functionality of DGs and topological changes [18–24], 4) suboptimal controller [22–24], 5) limitations to the decision variables [22–24], 6) high-order controllers [18], 7) centralized control structure [18,19], 8) non-robustness to several different subsequent changes [23,24], and 9) being inapplicable to DC microgrids with general topology [17,20,25].

This paper present an optimal robust primary voltage control approach for islanded uncertain DC microgrid with general structure. Each DG unit comprises a local uncertain ZIP load through a DC/DC converter, which can be different types, such as buck and boost. The proposed controller, opposed to works in [22–24], is based on the output-feedback, and unlike [18], has a fully decentralized structure, which offers several advantages, including lower communication bandwidth, availability of a proprietary control unit, fewer sensors, less computational burden, cost-effectiveness, and higher reliability. The main contribution of the proposed controller are as follows:

- The main focus of the presented voltage control scheme, unlike most of the previously proposed robust non-droop-based controllers [22–24], is on the robust desired performance (transient and steady-state) satisfaction in addition to robust voltage stabilization in the islanded DC microgrids with a general structure by providing a decentralized H_∞ fixed-order local voltage control strategy.
- The proposed controller guarantees robust stability and performance of the closed-loop microgrid system under several sources of uncertainty, including topology changes, uncertain ZIP loads, unknown load dynamics, PnP operations of DGs, and several subsequent changes caused by different mentioned uncertainty sources, by modeling all uncertainty sources as a new unique polytope.
- Unlike the proposed robust control schemes in [22–24], every local controller is a solution of a unique convex optimization problem, resulting in optimal performance and robustness to several different consecutive changes in addition to less computational complexity. More precisely, if any of the changes mentioned above occur, the closed-loop system is still robust to all sources of uncertainty.
- To achieve a decentralized control structure, contrary to the works in [22–24], which are based on the neutral interactions idea, the interaction terms between DG subsystems are modeled as a disturbance input with no constraint on the structure of final decision variables, which results in less conservatism.
- The robust controller design process is scalable, i.e., the local control system design for each DG unit is not dependent on the other DGs.

To attain these objectives, an average LTI state-space model is extracted for each DG unit, considering two disturbances from interaction inputs and unknown load dynamics. Next, the uncertain loads, the PnP operation of DGs, and the topological alterations are modeled as a new polytopic-type uncertainty. The design objectives are converted into an LMI description of a fixed-order dynamic output-feedback controller for a polytopic LTI state-space system. In order to evaluate its effectiveness by several case studies, the suggested control manner is exerted to a DC microgrid system, including 6 DGs [23]. The generated outcomes emphasize the efficiency of the presented controller in assuring robust stability and robust desirable performance. It should be noted that in this paper the robust stability and robust performance specifications are described in frequency-domain, which allows system design, control parameters adjustment, stability analysis, and performance studies to be done easily. Moreover, the frequency-domain conditions can be

transformed into time-domain, which helps to establish an effective control design [27]. For example, high closed-loop bandwidth provides a fast dynamic response.

Different sections of this paper are classified as follows: The mathematical model of the islanded DC microgrid system is obtained in Section 2. Section 3 presents the design process of the control system strategy. Simulation results are presented in Section 4, and the conclusions are given in Section 5.

All over the manuscript, the set of real numbers is indicated by . Matrices I and 0 show the identity and the zero matrices, respectively. The symbols P^T and $*$ indicate the matrix transpose and a symmetric block, respectively. For a symmetric matrix P, the relations $P < 0$ and $P > 0$ represent that the matrix is negative-definite and positive-definite, respectively. For a transfer function $T(s)$, the variable s is the complex Laplace variable, the symbol $\|T(s)\|_\infty$ indicates the value of the H_∞-norm, and the H_∞-norm is defined as the supremum (least upper bound) over all real-valued frequencies for the maximum singular value of the matrix.

2. Modeling of the islanded DC microgrids

Consider an islanded DC microgrid with the general structure, containing N DGs. Every DG unit consist of an ideal DC voltage source, a DC/DC converter, and a local uncertain ZIP load. First, a microgrid system comprising of two DGs, DG i and DG j, connected through a distribution line ij, is considered as depicted in Fig. 1. Depending on the application and the voltage level at the source and load sides, different types of converters, such as boost and buck, can be used in a DC microgrid. The average electrical model of the buck and boost converters are shown in Fig. 2. In the case of using other types of converters, e.g., cuk-type, the proper electrical model needs to be replaced, then the dynamic equations and the final state-space model must be extracted in accordance with the new electrical circuit and new dynamics. The description of the used symbols are given in Table 1. First, it is assumed that the DC-DC converters are buck-type with the average model shown in Fig. 2(a). The dynamic equations of the system, using the Kirchhoff's circuit laws, are as follows:

$$DG\ \ i: \begin{cases} \frac{dV_i}{dt} = \frac{1}{C_{ti}} I_{ti} - \frac{1}{C_{ti}} \hat{I}_{L_i} + \frac{1}{C_{ti}} I_{ij} \\ \frac{dI_{ti}}{dt} = -\frac{1}{L_{ti}} V_i - \frac{R_{ti}}{L_{ti}} I_{ti} + \frac{d_i}{L_{ti}} V_{si} \end{cases} \tag{1}$$

$$Line\ \ ij: \frac{dI_{ij}}{dt} = -\frac{R_{ij}}{L_{ij}} I_{ij} + \frac{1}{L_{ij}} V_j - \frac{1}{L_{ij}} V_i \tag{2}$$

$$Load\ \ i: \hat{I}_{L_i} = \frac{V_i}{Z_{li}} + I_{li} + \frac{P_{li}}{V_i},\ with\ Z_{li} \in \quad \geq 0 \tag{3}$$

By assuming that the distribution lines are Quasi-Stationary Line (QSL) [28], i.e. $\frac{dI_{ij}}{dt} = 0$, the line dynamic in (2) is rewritten as follows:

$$I_{ij} = (V_j - V_i)/R_{ij} \tag{4}$$

Since the impedance of the lines in the DC network is often resistive, the assumption of QSL is reasonable. By replacing the values of $\hat{I}_{L_i}$ and I_{ij} in the system equations (1), the dynamic of DG i is obtained as follows:

$$\begin{cases} \frac{dV_i}{dt} = \frac{1}{C_{ti}} \left(-\frac{V_i}{Z_{li}} - \frac{V_i}{R_{ij}} - \frac{P_{li}}{V_i} + I_{ti} - I_{li} + \frac{V_j}{R_{ij}} \right) \\ \frac{dI_{ti}}{dt} = \frac{1}{L_{ti}} (-V_i - R_{ti} I_{ti} + d_i V_{si}) \end{cases} \tag{5}$$

Assuming that the system (5) has an equilibrium, there exist constant signals $(V_{i_0}, V_{j_0}, I_{ti_0}, I_{li_0}, d_{i_0})$ such that:

$$\begin{cases} 0 = \frac{1}{C_{ti}} \left(-\frac{V_{i_0}}{Z_{li}} - \frac{V_{i_0}}{R_{ij}} - \frac{P_{li}}{V_{i_0}} + I_{ti_0} - I_{li_0} + \frac{V_{j_0}}{R_{ij}} \right) \\ 0 = \frac{1}{L_{ti}} (-V_{i_0} - R_{ti} I_{ti_0} + d_{i_0} V_{si}) \end{cases} \tag{6}$$

From the linearization of (5) around the constant signals $(V_{i_0}, V_{j_0}, I_{ti_0}, I_{li_0}, d_{i_0})$, the linearized model is obtained as follows:

$$\begin{cases} \frac{d\tilde{V}_i}{dt} = \frac{1}{C_{ti}} \left(-\frac{\tilde{V}_i}{Z_{li}} - \frac{\tilde{V}_i}{R_{ij}} + \frac{P_{li}}{V_{i_0}^2} \tilde{V}_i + \tilde{I}_{ti} - \tilde{I}_{li} + \frac{\tilde{V}_j}{R_{ij}} \right) \\ \frac{d\tilde{I}_{ti}}{dt} = \frac{1}{L_{ti}} (-\tilde{V}_i - R_{ti} \tilde{I}_{ti} + \tilde{d}_i V_{si}) \end{cases} \tag{7}$$

where $\tilde{V}_i = V_i - V_{i_0}$, $\tilde{V}_j = V_j - V_{j_0}$, $\tilde{I}_{ti} = I_{ti} - I_{ti_0}$, $\tilde{I}_{li} = I_{li} - I_{li_0}$, and $\tilde{d}_i = d_i - d_{i_0}$.

Likewise, if the DC microgrid system includes N DGs, and DG i is connected to a subset of DG units which comprises n_i DGs in the form $N_i = \{j_1, j_2, ..., j_{n_i}\} \subset \{1, ..., N\}$, the linearized dynamics of DG i are as follows:

$$\begin{cases} \frac{d\tilde{V}_i}{dt} = \frac{1}{C_{ti}} \left(-\frac{\tilde{V}_i}{Z_{li}} + \frac{P_{li}}{V_{i_0}^2} \tilde{V}_i - \sum_{j \in N_i} \frac{\tilde{V}_i}{R_{ij}} + \tilde{I}_{ti} - \tilde{I}_{li} + \sum_{j \in N_i} \frac{\tilde{V}_j}{R_{ij}} \right) \\ \frac{d\tilde{I}_{ti}}{dt} = \frac{1}{L_{ti}} (-\tilde{V}_i - R_{ti} \tilde{I}_{ti} + \tilde{d}_i V_{si}) \end{cases} \tag{8}$$

Therefore, the state-space equations for every DG in the autonomous mode are obtained in the following form:

$$\begin{cases} \dot{x}_i = A_{ii} x_i + B_{ii} u_i + B_{w_{1i}} w_{1i} + \sum_{k=1}^{n_i} A_{ij_k} \tilde{V}_{j_k} \\ y_i = C_{ii} x_i; \end{cases} \tag{9}$$

where $x_i = [\tilde{V}_i \ \ \tilde{I}_{ti}]^T$ is the state vector, $u_i = \tilde{d}_i V_{si}$ is the input, $\tilde{V}_j$ is the voltage of PCC j, $y_i = \tilde{V}_i$ is the output of DG i, n_i is the number of neighbors of DG i, $w_{1i} = \tilde{I}_{li}$ is the first exogenous input corresponding to the constant current load (CCL) changes and/or other unknown load dynamics, and the state-space matrices are as follows:

$$A_{ii} = \begin{bmatrix} \frac{1}{C_{ti}} \left(-\frac{1}{Z_{li}} + \frac{P_{li}}{V_{i_0}^2} - \sum_{k=1}^{n_i} \frac{1}{R_{ij_k}} \right) & \frac{1}{C_{ti}} \\ -\frac{1}{L_{ti}} & -\frac{R_{ti}}{L_{ti}} \end{bmatrix}, \ B_{ii} = \begin{bmatrix} 0 \\ \frac{1}{L_{ti}} \end{bmatrix}, \ B_{w_{1i}} = \begin{bmatrix} -\frac{1}{C_{ti}} \\ 0 \end{bmatrix}, \ A_{ij_k} = \begin{bmatrix} \frac{1}{C_{ti} R_{ij_k}} \\ 0 \end{bmatrix}, \ C_{ii} = [1 \ \ 0] \tag{10}$$

It should be noted that, in this model, $A_{ij_k} \tilde{V}_{j_k}$ is the interaction efficacy of subsystem j_k (kth neighbor of DG i) on subsystem i, and $A_{ij_k} = 0$ if and only if no connection among DGs i and j_k exists.

Now, it is assumed that the DC-DC converters are boost-type with the general model shown in Fig. 2(b). The dynamic equations of DG i,

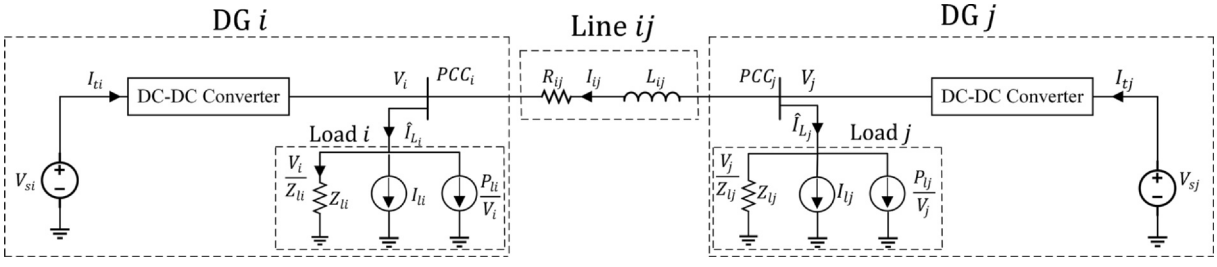

Fig. 1. General electrical diagram of a DC microgrid consists of two DGs connected via line ij.

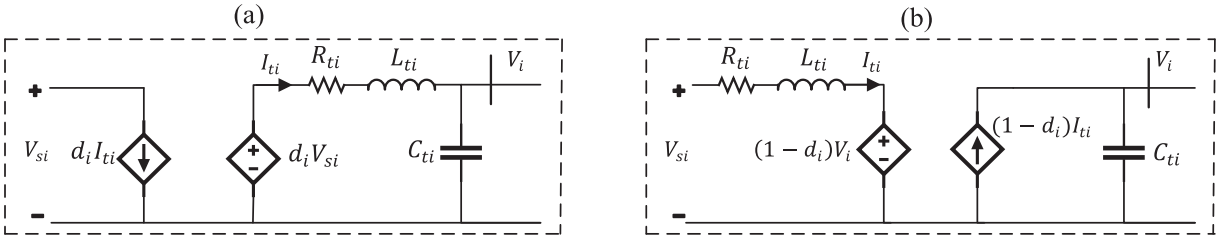

Fig. 2. Average model of a DC/DC converter: (a) model of a buck converter, and (b) model of a boost converter.

Table 1
Description for the used symbols.

Symbol	Description
V_{si}	Generated Voltage
V_i	Load Voltage
I_{ti}	Filter Current
$\hat{I}_{Li}$	Load Current
I_{ij}	Distribution Line Current
R_{ti}	Filter Resistance
L_{ti}	Filter Inductance
C_{ti}	Filter Capacitor
R_{ij}	Line Resistance
L_{ij}	Line Inductance
Z_{li}	Impedance of CIL
I_{li}	Current of CCL
P_{li}	Power of CPL
d_i	Duty Cycle of Converter

assuming that DG i is connected to a subset of DG units in the form N_i, are as follows:

$$\begin{cases} \frac{dV_i}{dt} = \frac{1}{C_{ti}}\left((1-d_i)I_{ti} - \left(\frac{V_i}{Z_{li}} + I_{li} + \frac{P_{li}}{V_i}\right) + \sum_{j\in N_i}\frac{V_j - V_i}{R_{ij}}\right) \\ \frac{dI_{ti}}{dt} = -\frac{1}{L_{ti}}((1-d_i)V_i - R_{ti}I_{ti} + V_{si}) \end{cases} \tag{11}$$

Due to the existence of the terms P_{li}/V_i, $(1-d_i)I_{ti}$, and $(1-d_i)V_i$, the system dynamical equations (11) are not linear. Linearization of this around operating fixed point $(V_{i_0}, V_{j_0}, I_{ti_0}, I_{Li_0}, d_{i_0})$ results in the following linear approximated model:

$$\begin{cases} \frac{d\tilde{V}_i}{dt} = \frac{1}{C_{ti}}\left(-\frac{\tilde{V}_i}{Z_{li}} + \frac{P_{li}}{V_{i_0}^2}\tilde{V}_i - \sum_{j\in N_i}\frac{\tilde{V}_i}{R_{ij}} + (1-d_{i_0})\tilde{I}_{ti} - I_{ti_0}\tilde{d}_i - \tilde{I}_{li} + \sum_{j\in N_i}\frac{\tilde{V}_j}{R_{ij}}\right) \\ \frac{d\tilde{I}_{ti}}{dt} = \frac{1}{L_{ti}}(-(1-d_i)\tilde{V}_i - R_{ti}\tilde{I}_{ti} + V_{i_0}\tilde{d}_i + \tilde{V}_{si}) \end{cases} \tag{12}$$

where $\tilde{V}_{si} = V_{si} - V_{si_0}$ is the small-signal input voltage disturbance, which can be neglected, since the input voltage changes are very slow.

The equations (12) are presented in the state-space model similar to (9), where $u_i = \tilde{d}_i$, and the state-space matrices are as follows:

$$A_{ii} = \begin{bmatrix} \frac{1}{C_{ti}}\left(-\frac{1}{Z_{li}} + \frac{P_{li}}{V_{i_0}^2} - \sum_{k=1}^{n_i}\frac{1}{R_{ij_k}}\right) & \frac{1-d_{i_0}}{C_{ti}} \\ -\frac{1-d_{i_0}}{L_{ti}} & -\frac{R_{ti}}{L_{ti}} \end{bmatrix}, \quad B_{ii} = \begin{bmatrix} \frac{-I_{ti_0}}{C_{ti}} \\ \frac{V_{i_0}}{L_{ti}} \end{bmatrix}, \quad B_{w_{1i}} = \begin{bmatrix} \frac{-1}{C_{ti}} \\ 0 \end{bmatrix}, \quad A_{ij_k} = \begin{bmatrix} \frac{1}{C_{ti}R_{ij_k}} \\ 0 \end{bmatrix}, \quad C_{ii} = [1 \;\; 0] \tag{13}$$

3. Control system strategy of DC microgrid

The presented voltage control strategy in this paper is hierarchical, comprising two principal levels with different time scales. The first level controller must stabilize the PCC voltage and provide the desirable performance indicators such as offset-free reference voltage tracking, robustly. The second level control, which is called the power management system (PMS), maintains the optimal operating point of the autonomous DC microgrid and transmits the voltage set-points to the initial level. The PMS centrally solves a power flow problem and sends the set points to the primary controllers of DG units. The structure of the proposed primary controller is fully decentralized. The major purpose of this paper is to develop a primary robust controller for autonomous DC microgrids with the general topology, and the main design objectives are as follows:

- Fully decentralized structure of the primary voltage controller
- Voltage stabilization of the closed-loop microgrid system
- Desired performance satisfaction of the overall closed-loop system, including limited transient response, reference tracking, zero steady-state voltage tracking error, and bounded control signal
- Robustness of stability and desirable performance of the closed-loop system versus topological changes, PnP functionalities of DGs, ZIP load variations, unknown load dynamics, and several different subsequent changes

Steps of the design process of the robust controller are discussed as follows:

3.1. Stage 1: Structure of the proposed voltage controller

In a decentralized control manner, the local control center for DG i must utilize only its local measurements to provide overall stability and desirable functionality. To hamper possible instability and weak performance due to the efficacies of interactions $\sum_{j\in N_i} A_{ij}V_j$, the interaction terms are regarded as a disturbance vector, as follows:

$$\begin{cases} \dot{x}_i = A_{ii}x_i + B_{ii}u_i + B_{w_{1i}}w_{1i} + B_{w_{2i}}w_{2i} \\ y_i = C_{ii}x_i; \qquad\qquad i = 1,...,N \end{cases} \tag{14}$$

where $w_{2i} = [V_{j_1}\, V_{j_2}...V_{j_{ni}}]^T$ is the second exogenous input and the matrix $B_{w_{2i}}$ is defined as follows:

$$B_{w_{2i}} = [A_{ij_1}A_{ij_2}...A_{ij_{ni}}] \tag{15}$$

Then, a robust local controller is planned, so that it dominates this disturbance. Actually, by minimizing the effect of exogenous input w_{2i} on the local measured output y_i via minimizing the H_∞ norm of the equivalent transfer function, the stability and desirable performance were retained, notwithstanding the existence of interaction terms. It is worth pointing out that, from the obtained DC microgrid mathematical model (1)–(15), the interactions $A_{ij}V_j$ are resulted from the PCC voltages. Therefore, the interaction terms are bounded and can be assumed as a bounded disturbance, if the closed-loop system is stable.

The initial control objectives for subsystem i (DG unit i) are, 1) stability, acceptable transient response, reference tracking, offset-free voltage tracking, and appropriate control input, and 2) attenuation of uncertain CCL disturbance and/or other unknown load dynamics. The first objective is attained by the appropriate design of a feedback controller $K_i(s)$. While, the second one is gained by measuring the load current and compensating its effect via a feedforward controller $K_{wi}(s)$. Fig. 3 shows the general scheme of the proposed non-droop-based control approach for islanded DC microgrid. The simultaneous design of

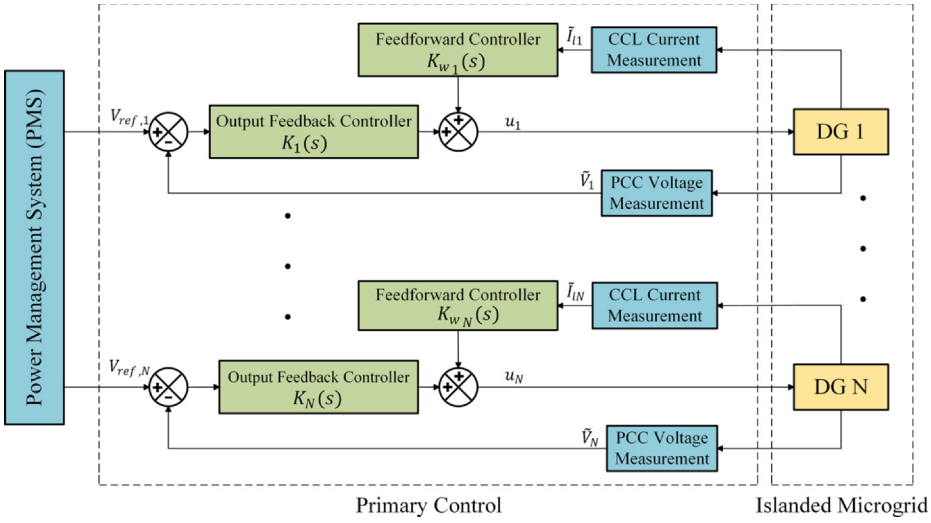

Fig. 3. Block diagram of the proposed voltage control approach.

the feedback and feedforward controllers for each DG subsystem is one of the main purposes.

3.2. Stage 2: Initial formulation for the controller design

Consider the block diagram of Fig. 4. The transfer functions $G_i(s)$, $G_{w1i}(s)$ and $G_{w2i}(s)$ are acquired from the state-space description of DG i, specified in (10), (13) and (15), as follows:

$$\begin{cases} G_i(s) = C_{ii}(sI - A_{ii})^{-1}B_{ii} \\ G_{w1i}(s) = C_{ii}(sI - A_{ii})^{-1}B_{w_{1i}} \\ G_{w2i}(s) = C_{ii}(sI - A_{ii})^{-1}B_{w_{2i}} \end{cases} \tag{16}$$

To convert all initial control objectives into a single optimization problem, the following steps are taken:

For the reference tracking, the effect of the reference input r_i on the error signal e_i must be decreased. This objective can be attained by minimizing the ratio of the L_2 norm of the error signal to the reference input via the following optimization problem:

$$\begin{aligned} min\left(\sup_{r_i\in\mathscr{L}_2}\frac{\|e_i\|_{L_2}}{\|r_i\|_{L_2}}\right) &= min\|T_{r_ie_i}\|_\infty = min\|(I + G_i(s)K_i(s))^{-1}\|_\infty \\ &= min\|S_i(s)\|_\infty \end{aligned} \tag{17}$$

For the appropriate amplitude of control input, the effect of the reference signal r_i on the control signal u_i must be decreased, by minimizing the H_∞ norm of the equivalent transfer function, as follows:

$$min\left(\sup_{r_i\in\mathscr{L}_2}\frac{\|u_i\|_{L_2}}{\|r_i\|_{L_2}}\right) = min\|T_{r_iu_i}\|_\infty = min\|K_i(s)(I + G_i(s)K_i(s))^{-1}\|_\infty \tag{18}$$

Reducing the impact of exogenous input ($\bar{w}_i = [w_{1i} \;\; w_{2i}]^T$) on the output signal y_i, can be achieved through the following optimization problem:

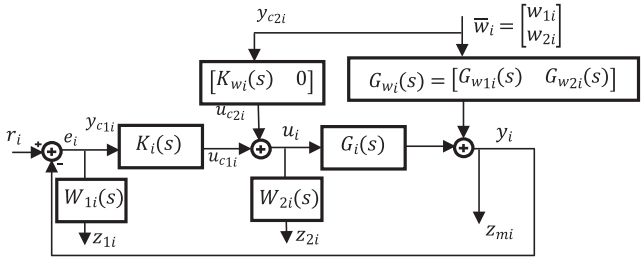

Fig. 4. Closed-loop block diagram for subsystem i.

problem:

$$\begin{aligned} min\left(\sup_{\bar{w}_i\in\mathscr{L}_2}\frac{\|y_i\|_{L_2}}{\|\bar{w}_i\|_{L_2}}\right) &= min\|T_{\bar{w}_iy_i}\|_\infty = min\|T_{w_{1i}y_i} \;\; T_{w_{2i}y_i}\|_\infty \\ &= min\left\|\begin{matrix}((I + G_i(s)K_i(s))^{-1}(G_{w1i} + G_iK_{wi}))^T \\ ((I + G_i(s)K_i(s))^{-1}G_{w2i})^T\end{matrix}\right\|_\infty \end{aligned} \tag{19}$$

Moreover, the proper weighing matrices $W_{1i}(s)$ and $W_{2i}(s)$ can be used in optimization problems (17) and (18), to adjust the bandwidth of the closed-loop system and the maximum of the sensitivity function, and to restrict the effect of the measurement noise and the control efforts, respectively, as shown in Fig. 4 [29].

Eventually, all control objectives can be formulated as the following optimization problem:

$$min_{K_i(s),K_{wi}(s)}\alpha_1\gamma_{1i} + \alpha_2\gamma_{2i}$$

$$s.\,t.\begin{cases}\left\|\begin{matrix}W_{1i}(s)S_i(s) \\ W_{2i}(s)K_i(s)S_i(s)\end{matrix}\right\|_\infty < \gamma_{1i} \\ \left\|\begin{matrix}(S_i(s)(G_{w1i}(s) + G_i(s)K_{wi}(s)))^T \\ (S_i(s)G_{w2i}(s))^T\end{matrix}\right\|_\infty < \gamma_{2i}\end{cases} \quad i = 1,...,N \tag{20}$$

where α_1 and α_2 are weighting factors that specify a trade-off between the disturbance signals attenuation and the H_∞ performance criterion.

3.3. Stage 3: The state-space representation for the constraints

The state-space models for the transfer functions appearing in the constraints of the optimization problem (20), are attained here. Considering the virtual diagram of Fig. 4, and using the state-space description of G_i, G_{wi}, W_{1i}, and W_{2i}, the state-space description of the augmented open-loop subsystem and desirable local controller $K_{Ci}(s) = [K_i(s) \;\; K_{wi}(s)]$ are respectively named as follows:

$$\begin{bmatrix}\dot{\hat{x}}_i \\ z_i \\ z_{mi} \\ y_i\end{bmatrix} = \begin{bmatrix}A_i & B_{ri} & B_{wi} & B_i \\ C_{zi} & D_{zri} & D_{zwi} & D_{zi} \\ C_{z_{mi}} & D_{z_{m}r_i} & D_{z_{m}w_i} & D_{z_{m}i} \\ C_i & D_{ri} & D_{wi} & 0\end{bmatrix}\begin{bmatrix}\hat{x}_i \\ r_i \\ \bar{w}_i \\ u_i\end{bmatrix} \tag{21}$$

$$\begin{cases}\dot{x}_{c_i} = A_{Ki}x_{c_i} + B_{Ki}y_{c_i} \\ u_i = C_{Ki}x_{c_i} + D_{Ki}y_{c_i}\end{cases} \tag{22}$$

where $z_i = [z_{1i} \;\; z_{2i}]^T$, and $y_{c_i} = [y_{c1i} \;\; y_{c2i}]^T$.

Now, the transfer function of the closed-loop DG subsystem is

defined as follows:

$$\begin{bmatrix} z_{1i} \\ z_{2i} \\ z_{mi} \\ y_{c1i} \\ y_{c2i} \end{bmatrix} = \begin{bmatrix} W_{1i} & -W_{1i}G_{w1i} & -W_{1i}G_{w2i} & -W_{1i}G_i \\ 0 & 0 & 0 & W_{2i} \\ 0 & G_{w1i} & G_{w2i} & G_i \\ I & -G_{w1i} & -G_{w2i} & -G_i \\ 0 & I & 0 & 0 \end{bmatrix} \begin{bmatrix} r_i \\ w_{1i} \\ w_{2i} \\ u_i \end{bmatrix} \tag{23}$$

Consequently, the state-space representation of the closed-loop subsystem i is attained as:

$$\begin{bmatrix} \dot{\hat{x}}_i \\ \dot{x}_{c_i} \end{bmatrix} = \begin{bmatrix} A_i + B_iD_{Ki}C_i & B_iC_{Ki} \\ B_{Ki}C_i & A_{Ki} \end{bmatrix} \begin{bmatrix} \hat{x}_i \\ x_{c_i} \end{bmatrix} + \begin{bmatrix} B_{ri} + B_iD_{Ki}D_{ri} & B_{wi} + B_iD_{Ki}D_{wi} \\ B_{Ki}D_{ri} & B_{Ki}D_{wi} \end{bmatrix} \begin{bmatrix} r_i \\ \bar{w}_i \end{bmatrix}$$

$$\begin{bmatrix} z_i \\ z_{mi} \end{bmatrix} = \begin{bmatrix} C_{zi} + D_{zi}D_{Ki}C_i & D_{zi}C_{Ki} \\ C_{z_{mi}} + D_{z_{mi}}D_{Ki}C_i & D_{z_{mi}}C_{Ki} \end{bmatrix} \begin{bmatrix} \hat{x}_i \\ x_{c_i} \end{bmatrix} + \begin{bmatrix} D_{zri} + D_{zi}D_{Ki}D_{ri} & D_{zwi} + D_{zi}D_{Ki}D_{wi} \\ D_{z_{mi}r_i} + D_{z_{mi}}D_{Ki}D_{ri} & D_{z_{mi}w_i} + D_{z_{mi}}D_{Ki}D_{wi} \end{bmatrix} \begin{bmatrix} r_i \\ \bar{w}_i \end{bmatrix} \tag{24}$$

Eventually, the state-space realization for constraints of the optimization problem (20) are as follows:

$$T_{r_iz_i}: \begin{bmatrix} \widehat{A}_i & \widehat{B}_{1i} \\ \widehat{C}_{1i} & \widehat{D}_{1i} \end{bmatrix} = \begin{bmatrix} \begin{pmatrix} A_i + B_iD_{Ki}C_i & B_iC_{Ki} \\ B_{Ki}C_i & A_{Ki} \end{pmatrix} & \begin{pmatrix} B_{ri} + B_iD_{Ki}D_{ri} \\ B_{Ki}D_{ri} \end{pmatrix} \\ (C_{zi} + D_{zi}D_{Ki}C_i \quad D_{zi}C_{Ki}) & D_{zri} + D_{zi}D_{Ki}D_{ri} \end{bmatrix} \tag{25}$$

$$T_{\bar{w}_iz_{mi}}: \begin{bmatrix} \widehat{A}_i & \widehat{B}_{2i} \\ \widehat{C}_{2i} & \widehat{D}_{2i} \end{bmatrix} = \begin{bmatrix} \begin{pmatrix} A_i + B_iD_{Ki}C_i & B_iC_{Ki} \\ B_{Ki}C_i & A_{Ki} \end{pmatrix} & \begin{pmatrix} B_{wi} + B_iD_{Ki}D_{wi} \\ B_{Ki}D_{wi} \end{pmatrix} \\ (C_{z_{mi}} + D_{z_{mi}}D_{Ki}C_i \quad D_{z_{mi}}C_{Ki}) & D_{z_mw_i} + D_{z_{mi}}D_{Ki}D_{wi} \end{bmatrix} \tag{26}$$

Therefore, the constraints representations (25) and (26) are equivalent to the closed-loop state-space description of an LTI system with a dynamic output-feedback controller. In what follows, after modeling the PnP operation of DGs, load variations, and topological changes as polytopic-type uncertainty, the final design problem is transformed into an LMI-based convex optimization problem.

3.4. Stage 4: Robustness to different sources of uncertainty

In this subsection, robustness of the closed-loop DC microgrid system under different sources of uncertainty, including PnP operations of DGs, local load variations, and topological changes, is investigated. The objective is to retain the stability and desirable performance of the overall microgrid system against these changes via proper modeling of uncertainties. To attain this, all uncertainty sources are modeled as a unique polytope in the state-space matrices proposed for the DC microgrid system in (10), (13), and (15). Then the final optimization problem will be satisfied at the vertices of the presented polytope.

3.4.1. PnP functionality of DGs

Conforming to the state-space matrices described in (10), (13), and (15), with plug-in/-out of each DG i, only the matrices A_{ii} and B_{w2i} for DG i and its neighboring DG units, change. In matrix A_{ii}, PnP functionalities only affect the first-row/first-column element ($a_{ii_{11}}$). Therefore, due to the effect of PnP operations, an interval uncertainty for this element is defined as follows:

$$q_{1i}^{min} \le q_{1i} = \sum_{k=1}^{n_i} \frac{1}{R_{ij_k}} \le q_{1i}^{max} \tag{27}$$

where the maximum and minimum values of q_{1i} are attained as follows:

- q_{1i}^{max}: Maximum possible connection of all neighboring DG units to DG i.
- q_{1i}^{min}: Disconnection of all neighbors connected to DG i and according to (10) and (13) $q_{1i}^{min} = 0$.

Besides, the changes in matrix B_{w2i} due to the PnP operations can be modeled as:

$$B_{w_{2i}} = [\lambda_1 A_{ij_1} \lambda_2 A_{ij_2} ... \lambda_{n_i} A_{ij_{n_i}}] \tag{28}$$

where $\lambda_k \in \{0, 1\}$, and $\lambda_k = 0$ due to the plugging out of the kth neighboring unit of DG i; otherwise, $\lambda_k = 1$.

In the control objectives outlined in Section 3.2, matrix B_{w2i} appears only in the $\|T_{w_{2i}y_i}\|_\infty < \gamma_{2i}$ constraint, and this constraint can be re-written as follows:

$$\|T_{w_{2i}y_i}\|_\infty = \left\| \lambda_1 T_{i,j_1} \quad \lambda_2 T_{i,j_2} \quad \cdots \quad \lambda_{n_i} T_{i,j_{n_i}} \right\|_\infty < \gamma_{2i} \tag{29}$$

where T_{i,j_k} is the transfer function from the output PCC voltage of the kth neighbor of DG i, i.e. V_{j_k}, to the output of DG i, i.e. y_i.

If the kth neighbor of DG i is plugged-out, then $\lambda_k = 0$. As a result, the corresponding transfer function (T_{i,j_k}) will be deleted in (29). Therefore, the constraint (29) changes as follow:

$$\left\| \lambda_1 T_{i,j_1} \quad \cdots \quad \lambda_{k-1} T_{i,j_{k-1}} \quad 0 \quad \lambda_{k+1} T_{i,j_{k+1}} \quad \cdots \quad \lambda_{n_i} T_{i,j_{n_i}} \right\|_\infty = \left\| T_{w_{2i}y_i} \times \begin{bmatrix} I_{k-1} & 0 & 0 \\ 0 & 0 & 0 \\ 0 & 0 & I_{n_i-k} \end{bmatrix}_{n_i \times n_i} \right\|_\infty \tag{30}$$

and the following conditions hold too:

$$\left\| T_{w_{2i}y_i} \times \begin{bmatrix} I_{k-1} & 0 & 0 \\ 0 & 0 & 0 \\ 0 & 0 & I_{n_i-k} \end{bmatrix}_{n_i \times n_i} \right\|_\infty \leqslant \underbrace{\|T_{w_{2i}y_i}\|_\infty}_{<\gamma_{2i}} \times \left\| \underbrace{\begin{bmatrix} I_{k-1} & 0 & 0 \\ 0 & 0 & 0 \\ 0 & 0 & I_{n_i-k} \end{bmatrix}}_{=1} \right\|_\infty < \gamma_{2i} \times 1 = \gamma_{2i} \tag{31}$$

Consequently, if the constraint (29) for DG i is met under maximum possible connections of other DGs to DG i, it will also be satisfied after the disconnections of some adjacent units. Therefore, it is sufficient to satisfy this constraint only in the case of the maximum possible interactions, i.e. $\lambda_k = 1$ for $k = 1, ..., n_i$. It should be noted that, if all the lines connected to DG i are detached (corresponding to q_{1i}^{min}), the matrix B_{w2i} will be zero.

Remark. The effect of changing matrix A_{ii} due to plugging in/out of its neighbors on the transfer functions T_{i,j_k} for $k = 1, ..., n_i$, has been considered via the proposed interval uncertainty in (27) and the polytope provided in the following.

3.4.2. Uncertain ZIP loads

On modeling uncertain constant impedance load (Z_{li}) and uncertain constant power load (P_{li}), the changes of these loads only affect the $a_{ii_{11}}$ element of matrix A_{ii}. By assuming that these loads belong to a given interval as follows:

$$Z_{li}^{min} \le Z_{li} \le Z_{li}^{max}, \quad P_{li}^{min} \le P_{li} \le P_{li}^{max} \tag{32}$$

the following ranges are obtained:

$$q_{2i}^{min} = \frac{1}{Z_{li}^{max}} \le q_{2i} = \frac{1}{Z_{li}} \le \frac{1}{Z_{li}^{min}} = q_{2i}^{max} \tag{33}$$

$$q_{3i}^{min} = \frac{P_{li}^{min}}{V_{i0}^2} \le q_{3i} = \frac{P_{li}}{V_{i0}^2} \le \frac{P_{li}^{max}}{V_{i0}^2} = q_{3i}^{max} \tag{34}$$

Therefore, according to (27), (33), and (34), a single interval uncertainty is obtained for the element $a_{ii_{11}}$ due to the PnP operations and uncertain loads, as follows:

$$a_{ii_{11}}^{min} \le a_{ii_{11}} = \frac{1}{C_{ti}}(-q_{1i} - q_{2i} + q_{3i}) \le a_{ii_{11}}^{max} \tag{35}$$

where

$$a_{ii_{11}}^{min} = \frac{1}{C_{ti}}(-q_{1i}^{max} - q_{2i}^{max} + q_{3i}^{min}),\ \ a_{ii_{11}}^{max} = \frac{1}{C_{ti}}(-q_{1i}^{min} - q_{2i}^{min} + q_{3i}^{max}) \tag{36}$$

Consequently, in the DC microgrid system, the PnP operations of DGs and the changes of uncertain loads can be modeled as a polytopic-type uncertainty with 2 vertices in state-space matrices B_{wi2} and A_{ii}, as follows:

$$(A_{ii}, B_{wi2})(\theta) = \theta(A_{ii}^1, B_{wi2}^1) + (1-\theta)(A_{ii}^2, B_{wi2}^2),\ \ 0 \le \theta \le 1 \tag{37}$$

where $(A_{ii}^j, B_{wi2}^j),\ j = 1, 2$ represents the system matrices related to the vertex j, which are obtained as follows:

$$A_{ii}^1 = \begin{bmatrix} a_{ii_{11}}^{min} & a_{ii_{12}} \\ a_{ii_{21}} & a_{ii_{22}} \end{bmatrix},\ \ B_{w2i}^1 = [A_{ij_1}A_{ij_2}...A_{ij_{ni}}],\ \ A_{ii}^2 = \begin{bmatrix} a_{ii_{11}}^{max} & a_{ii_{12}} \\ a_{ii_{21}} & a_{ii_{22}} \end{bmatrix},\ \ B_{w2i}^2 = 0 \tag{38}$$

3.4.3. Microgrid topology changes

Since all of the possible scenarios for connection or disconnection of the DG units are considered in the polytopic modeling of PnP operations in matrices A_{ii} and B_{wi2}, the disconnection of some distribution lines between DG units is not affected the polytopic uncertainty domain and its vertices. Consequently, the polytopic zone considered for the modeling of PnP functionalities and uncertain ZIP loads also includes robustness to topological changes due to PnP, link failures, etc. Therefore, the proposed approach and the presented polytopic space are also robust to the microgrid topology changes.

Therefore, the dynamics of a DG under different mentioned sources of uncertainty are described by the following polytopic state-space model:

$$\begin{cases} \dot{x}_i = A_{ii}(\theta)x_i + B_{ii}u_i + B_{w_{1i}}w_{1i} + B_{w_{2i}}(\theta)w_{2i} \\ y_i = C_{ii}x_i; \end{cases} \tag{39}$$

It should be noted that the polytopic uncertain matrices A_{ii} and B_{w2i} result in polytopic uncertainty in the open-loop augmented state-space matrices A_i, B_{wi}, D_{wi}, D_{zwi} and $D_{z_mw_i}$ for each DG subsystem described in (21).

3.5. Stage 5: Convex description for the final problem

Pursuant to the outcomes of the prior parts, the final problem is to design the dynamic output-feedback controller with H_∞ performance criterion for LTI polytopic state-space systems. The design must be accomplished via solving a unique convex LMI-based optimization problem in the convex hull vertices. In the obtained LMIs, if there is no coupling between the Lyapunov matrix and the system state-space matrices, the possibility of using the linearly parameter-dependent (LPD) Lyapunov function is created instead of the common Lyapunov matrix. It is thereby reducing the conservatism in robust controller design for the entire polytopic uncertain zone. Therefore, an iterative algorithm is proposed here to solve this nonconvex optimization problem using the LPD Lyapunov function via a fixed-order controller. The presented method is used to design a robust reduced-order dynamic output-feedback controller for the islanded DC microgrid system.

Consider the LTI system H indicated by the following equations,

$$H: \begin{cases} \dot{x} = Ax + B_w w + Bu \\ z = C_z x + D_{zw} w + D_z u \\ y = Cx + D_w w \end{cases} \tag{40}$$

where x is the state vector, u is the control input, y is a vector of the measured outputs, w is a vector of exogenous inputs, and z is a vector of output signals corresponding to the desirable performance of the closed-loop system.

It is assumed that the state-space matrices be included in a polytopic uncertainty region with q vertices as follows:

$$\begin{bmatrix} A(\theta) & B_w(\theta) & B(\theta) \\ C_z(\theta) & D_{zw}(\theta) & D_z(\theta) \\ C(\theta) & D_w(\theta) & 0 \end{bmatrix} = \sum_{j=1}^{q} \theta_j \begin{bmatrix} A^j & B_w^j & B^j \\ C_z^j & D_{zw}^j & D_z^j \\ C^j & D_w^j & 0 \end{bmatrix} \tag{41}$$

where matrices $(A^j, B_w^j, B^j, C^j, C_z^j, D_z^j, D_{zw}^j, D_w^j)$ represent the jth vertex of the polytope, and $\theta = [\theta_1 ... \theta_q]^T$ belongs to the following unit simplex,

$$\left\{ \theta \in \ ^q : \sum_{j=1}^{q} \theta_j = 1,\ \theta_j \ge 0 \right\} \tag{42}$$

After the utilization of the dynamic output-feedback controller $K(s)$: $\begin{bmatrix} A_K & B_K \\ C_K & D_K \end{bmatrix}$, the state-space representation of the closed-loop system is as follows:

$$T_{wz}(\theta): \begin{bmatrix} A_{cl}(\theta) & B_{cl}(\theta) \\ C_{cl}(\theta) & D_{cl}(\theta) \end{bmatrix} = \begin{bmatrix} \begin{pmatrix} A(\theta) + B(\theta)D_K C(\theta) & B(\theta)C_K \\ B_K C(\theta) & A_K \end{pmatrix} & \begin{pmatrix} B_w(\theta) + B(\theta)D_K D_w(\theta) \\ B_K D_w(\theta) \end{pmatrix} \\ (C_z(\theta) + D_z(\theta)D_K C(\theta) \quad D_z(\theta)C_K) & D_{zw}(\theta) + D_z(\theta)D_K D_w(\theta) \end{bmatrix} \tag{43}$$

To hold the linear dependency of the closed-loop state-space matrices on the vector θ, and since in the state-space description of constraints proposed in (25) and (26) only the matrices A_i, B_{wi}, D_{wi} and $D_{z_mw_i}$ are uncertain, it is supposed that matrices B and D_z are constant. The robust fixed-order dynamic output-feedback controllers are designed via the following Theorems.

Theorem 1. *Suppose that matrix M is given, then the system (A, B, C, D) is stable, and the inequality $\|C(SI - A)^{-1}B + D\|_\infty < \gamma$ holds, if there exists a scalar $\beta \gg 1$ and symmetric Lyapunov matrix $P = P^T > 0$ such that:*

$$\begin{bmatrix} -(M^T + M) & P + M^T A & M^T B & 0 & M^T \\ P + A^T M & -\beta P & 0 & C^T & 0 \\ B^T M & o & -\gamma I & D^T & 0 \\ 0 & C & D & -\gamma I & 0 \\ M & 0 & 0 & 0 & -\beta^{-1}P \end{bmatrix} < 0 \tag{44}$$

Proof. See Appendix A.

Now, the robust polytope expansion of Theorem 1 can be described as follows:

Theorem 2. *Suppose that matrix M is given, then the fixed-order controller $K(s)$: $\begin{bmatrix} A_K & B_K \\ C_K & D_K \end{bmatrix}$ guarantees the robust stability and the robust performance $\|T_{wz}(\theta)\|_\infty < \gamma$ of the closed-loop system (43) for all the systems in the polytopic set provided by (41), if there exists a scalar $\beta \gg 1$ and symmetric Lyapunov matrices $P^j = P^{jT} > 0$ such that for $j = 1, ..., q$:*

$$f^j\left(\begin{matrix} A^j,\ B,\ C^j,\ B_w^j,\ C_z^j,\ D_w^j,\ D_Z,\ D_{zw}^j, M,\ \beta| \\ A_K,\ B_K,\ C_K,\ D_K,\ P^j,\ \gamma \end{matrix}\right) = \begin{bmatrix} -(M+M^T) & P^j + M^T A_{cl}^j & M^T B_{cl}^j & 0 & M^T \\ * & -\beta P^j & 0 & C_{cl}^{jT} & 0 \\ * & * & -\gamma I & D_{cl}^{jT} & 0 \\ * & * & * & -\gamma I & 0 \\ * & * & * & * & -\beta^{-1} P^j \end{bmatrix} < 0 \tag{45}$$

where the sign | is the arguments of f^j disconnects the known parameters and the decision variables.

Proof. See Appendix B.

Remarks.

- An iterative algorithm is required to solve the problem of robust fixed-order H_∞ controller design presented in (45). First, for an initial controller and a fixed scalar β, matrix M is computed from the optimization problem (45). Then, the controller is redesigned by Theorem 2 using the obtained auxiliary matrix M. Now, the obtained controller is used as an initial controller to recalculate M. This process terminates on convergence (a priori defined tolerance for γ) or achieving the maximum iterations number (h_{max}).
- The initial controller can be calculated for each vertex of the polytope by the HIFOO method proposed in [30].
- Since, the auxiliary matrix and the state-space matrices of the controller are computed from one optimization problem, the upper bound on the H_∞ performance (γ) during the iterations is decreasing. Therefore, it can be easily indicated that the fixed-order controller design process propels to a monotonic convergence of the H_∞ norm upper bound.

Based on the consequences of Theorem 2, the ultimate design problem of the local voltage controller for every DG subsystem in autonomous general-structure DC microgrids with robust desirable performance and robust stability, can be expressed as a multi-objective convex optimization problem via satisfying a set of LMI constraints at the vertices of the proposed polytope as follows:

$$min_{P_{1i}^j, P_{2i}^j, A_{Ki}, B_{Ki}, C_{Ki}, D_{Ki}, M_{1i}, M_{2i}}\ \alpha_1\gamma_{1i} + \alpha_2\gamma_{2i}$$

subject to:

$$f^j\left(\begin{matrix} A_i^j,\ B_i,\ C_i,\ B_{ri},\ C_{zi},\ D_{zi},\ D_{ri},\ D_{zri},\ M_{1i},\ \beta_{1i}| \\ A_{Ki},\ B_{Ki},\ C_{Ki},\ D_{Ki},\ P_{1i}^j,\ \gamma_{1i} \end{matrix}\right) < 0$$

$$f^j\left(\begin{matrix} A_i^j,\ B_i,\ C_i,\ B_{w_i}^j,\ C_{z_m i},\ D_{z_m i},\ D_{w_i}^j,\ D_{z_m w_i}^j,\ M_{2i},\ \beta_{2i}| \\ A_{Ki},\ B_{Ki},\ C_{Ki},\ D_{Ki},\ P_{2i}^j,\ \gamma_{2i} \end{matrix}\right) < 0$$

$$P_{1i}^j > 0,\ \ P_{2i}^j > 0 \qquad j = 1, 2. \tag{46}$$

3.5.1. Robust decentralized controller design algorithm

The final design process of the robust local controller for every DG subsystem consists of the following steps:

Step 1: Create matrices A_{ii}, B_{ii}, B_{w1i}, B_{w2i} and C_{ii}, given in (10), (13) and (15), and then, the state-space matrices of augmented open loop subsystems pursuant to (21) for $i = 1, ..., N$.
Step 2: Create vertices of polytopic uncertain matrices (A_{ii}^j, B_{w2i}^j), according to (38) and then, extract the vertices of $(A_i^j, B_{w_i}^j, D_{w_i}^j, D_{z_m w_i}^j)$ according to (21) for $j = 1, 2$.
Step 3: Find the initial controller for each vertex of the polytope.
Step 4: Solve the LMI-based optimization problem (46) to extract the final robust local controller $K_{Ci}(s)$.
Step 5: Elicit the state-space description of feedback controller $K_i(s)$ and feedforward controller $K_{w_i}(s)$.

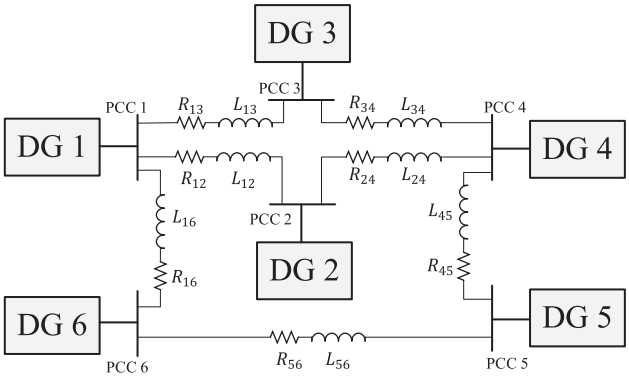

Fig. 5. Plan of the test DC microgird system composed of 6 DGs.

4. Simulation results

The effectiveness of the suggested control scheme is evaluated under various simulation scenarios. We use an autonomous DC microgrid, which includes 6 DGs with different types of converter, as depicted in Fig. 5. The electrical parameters of DGs and distribution lines are specified in Table 2. All simulation case studies were performed on a computer with an Intel Core i5-540 M (2.53 GHz), 4-GB RAM (532 MHz), and Windows 7. The local robust voltage controllers are acquired using the final five-step algorithm presented in Section 3.5.1, and the convex optimization problem (46) is solved in MATLAB/YALMIP [31]. The test microgrid system is simulated in SimPowerSystems Toolbox of MATLAB. Robust stability, robust desired transient and robust steady-state desirable performance of the DC system in Fig. 5 with the designed controller are verified by a class of general test, including performance of the nominal system and performance under PnP operations of DGs, load variations and microgrid topology changes.

4.1. Performance of the nominal closed-loop system

In this case study, stability and desirable performance of the

Table 2
Parameters of the test DC microgrid.

Electrical Parameters of DGs						
DG	CONVERTER TYPE	$R_{li}(\Omega)$	$L_{li}(mH)$	$C_{li}(mF)$	$V_{ref,i}(V)$	$V_{si}(V)$
1	Buck	0.2	1.8	2.2	47.9	100
2	Buck	0.3	2.0	1.9	48	100
3	Buck	0.1	2.2	1.7	47.7	100
4	Boost	0.5	3.0	2.5	48	25
5	Buck	0.4	1.2	2.0	47.8	100
6	Buck	0.6	2.5	3.0	48.1	100
Parameters of Local Loads						
DG	$Z_{li}(\Omega)$		$I_{li}(A)$		$P_{li}(W)$	
1	10 ($\pm5\Omega$)		0		300($\pm100W$)	
2	6 ($\pm4\Omega$)		0		350($\pm100W$)	
3	20 ($\pm10\Omega$)		0		0	
4	3 ($\pm2\Omega$)		0		0	
5	6 ($\pm4\Omega$)		11($\pm3A$)		0	
6	7.5 ($\pm5\Omega$)		3($\pm2A$)		0	
Parameters of Distribution Lines						
Line ij	$R_{ij}(\Omega)$		$L_{ij}(\mu H)$			
Line 12	0.05		2.1			
Line 13	0.07		1.8			
Line 34	0.06		1.0			
Line 24	0.04		2.3			
Line 45	0.08		1.8			
Line 16	0.1		2.5			
Line 56	0.08		3.0			

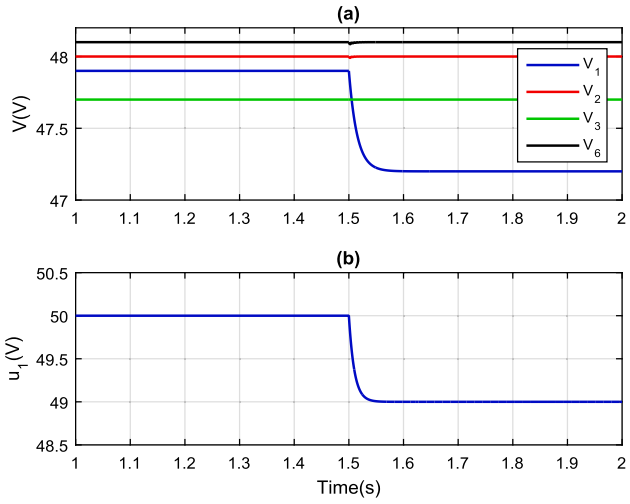

Fig. 6. Dynamic response of nominal microgrid under the reference voltage changes of DG 1 at $t = 1.5s$: (a) PCC voltage signals of DG 1 and its neighboring DGs, and (b) control signal of DG 1.

nominal closed-loop system are investigated. Initially, the voltage references for all DGs are adjusted pursuant to Table 2. Then, the PCC 1 voltage reference is varied to $47.2V$ at $t = 1.5s$. The output voltages of DG 1 and its neighbors, and control signal of DG 1 are shown in Fig. 6(a) and (b), respectively. The results illustrate that the proper tracking of the reference signal with a fast and limited transient response and zero steady-state error in less than $0.05s$ that is acceptable regarding the IEEE standards [32]. Also, Fig. 6(b) indicates that the magnitude of the control signal is always suitable. The obtained consequences from this scenario demonstrate that the provided controller guarantees the stability and desirable performance of the closed-loop nominal DC microgrid and is robust with respect to the reference signals variations.

4.2. Performance under PnP operations of DGs

In this part, robust stability and robust performance of the closed-loop system with the proposed controller under PnP operations are evaluated. To this end, it is supposed that DG 5 is plugged out from the test system at $t = 1s$, and again plugged back into the microgrid at $t = 1.8s$. Due to this PnP occurrence, all the distribution lines joint to DG 5 are disconnected in the time interval $t = 1s$ to $t = 1.8s$. Thus, the dynamics of DGs 4 and 6 are affected. Fig. 7 displays the dynamic voltage outputs of DG 5 and its neighboring DGs under these changes. The consequences demonstrate that the stability and desirable performance of the islanded DC microgrid are retained versus the PnP functionalities of DGs, and the designed local controllers adjust the PCC voltages after the PnP operations with zero steady-state error and a fast and acceptable transient response [32]. In other words, the proposed decentralized controller is robust to the PnP operations of DG units, not requiring retune of the local voltage controllers.

4.3. Robustness to topology changes

In this part, the robustness of the proposed local controllers against topological change is tested. To this end, Line 12 and Line 16 are disconnected at $t = 1s$ and $t = 1.2s$, respectively. Therefore, topology of the test DC microgrid in Fig. 6 is converted into the configuration displayed in Fig. 8. The dynamic voltage outputs of all DGs to these topological changes are shown in Fig. 9. The obtained outcomes indicate that the local controllers can regulate the PCC voltages quickly with zero steady-state error and preserve the stability and the desirable performance of the closed-loop test microgrid after the major changes in its

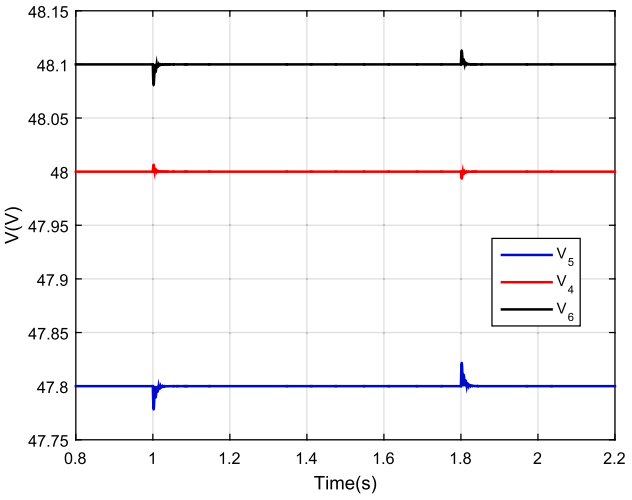

Fig. 7. PCC voltage signals of DG 5 and its neighboring DGs due to the PnP functionality of DG 5.

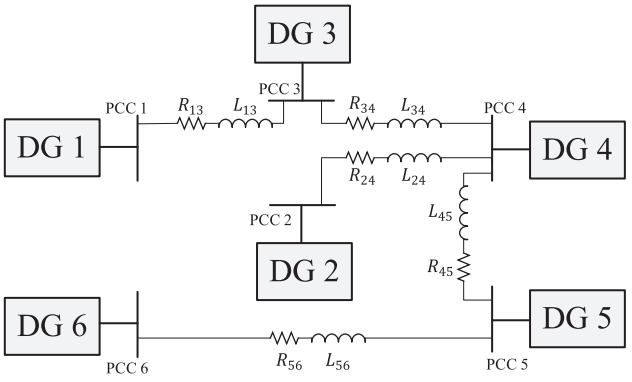

Fig. 8. Configuration of the autonomous DC microgrid after topology change.

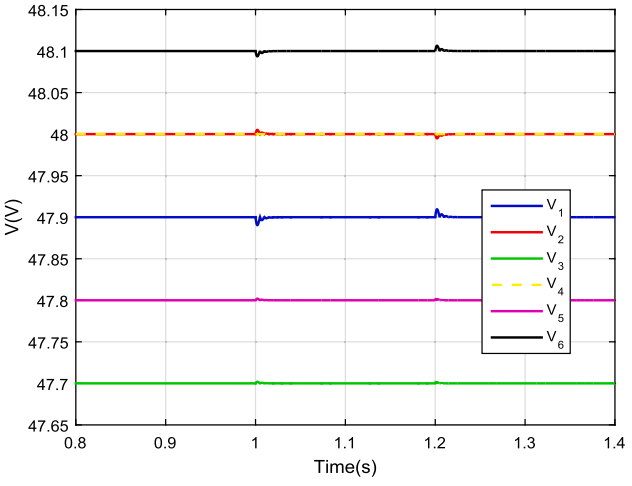

Fig. 9. PCC voltage signals of all DGs under the topological changes at $t = 1s$ and $t = 1.2s$.

configuration. Thus, the proposed controller is robust versus uncertainties that change the microgrid topology.

4.4. Robustness to uncertain constant power loads

In this scenario, the robustness of the closed-loop test microgrid with the designed decentralized controller to the changes of CPLs is verified. Hence, the power of CPL of DG 1 is altered in the defined

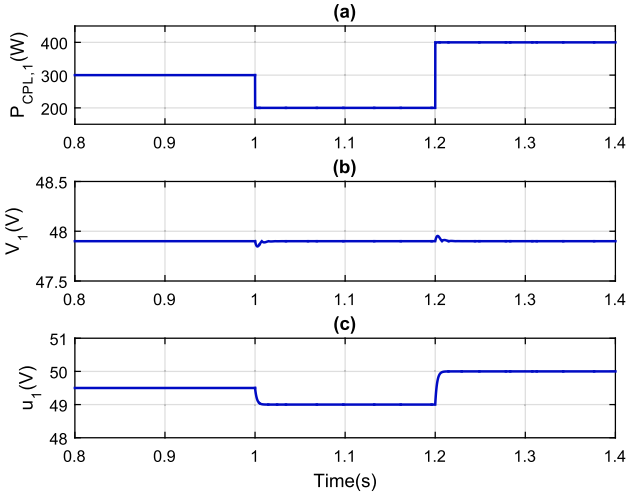

Fig. 10. DG 1 dynamic response due to the changes in CPL: (a) power of CPL, (b) PCC voltage, and (c) control signal.

range, according to Fig. 10(a). The voltage signal of PCC 1 and the control signal of DG 1 are displayed in Fig. 10(b) and (c), respectively. According to the attained results, the desired performance and stability of the DC microgrid system is robust against the uncertain CPLs.

4.5. Robustness to uncertain constant impedance loads

The purpose of this test is to verify the robustness of the microgrid system with respect to CIL changes. Therefore, the load resistance at PCC 6 is changed from 7.5Ω to 5Ω at $t = 0.9s$. Fig. 11(a) shows the PCC voltages of DG 6 and its neighboring DGs due to this change. The control signal of DG 6 is given in Fig. 11(b). The results demonstrate that, after a short transient, the stability and desirable performance of the closed-loop DC microgrid are maintained under impedance load changes and the designed controller is strongly robust.

4.6. Robustness to uncertain constant current loads

This case study evaluates the robustness of the closed-loop system to the CCL uncertainty. Therefore, the load current at PCC 5 is stepped down from 11A to 9A at $t = 0.9s$. PCC voltage signal and control input of DG 5 are shown in Fig. 12(a) and (b), respectively. The outcomes show

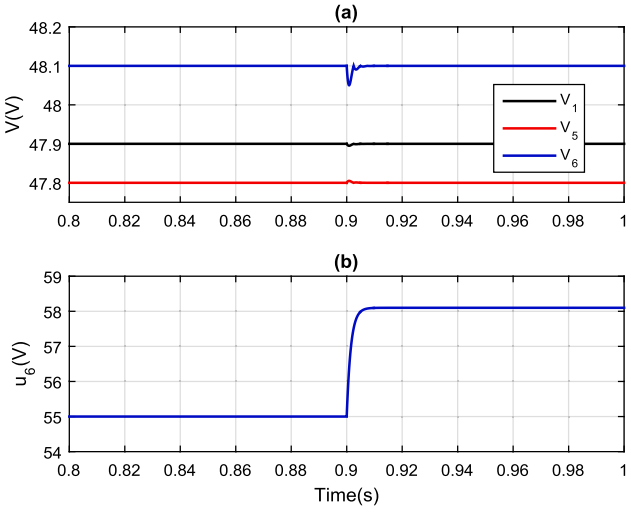

Fig. 11. Dynamic responses of DG 6 and its neighbors due to constant impedance load change of PCC 6 at $t = 0.9s$: (a) PCC voltage signal of DG 6 and its neighbours, (b) control signal of DG 6.

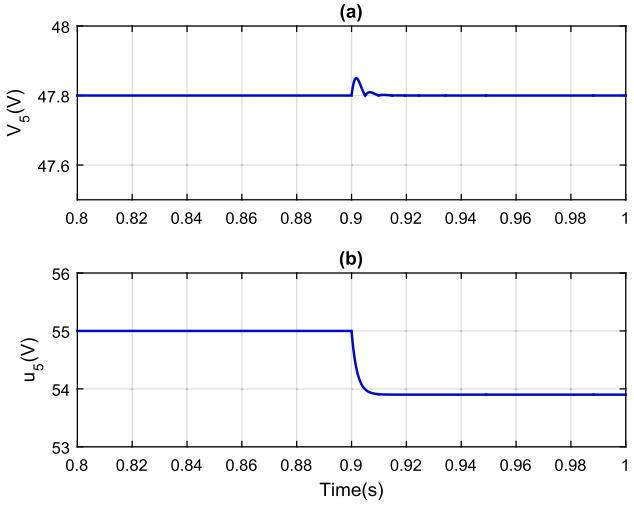

Fig. 12. DG 5 dynamic response due to constant current load change at $t = 0.9s$: (a) PCC voltage, (b) control signal.

that the closed-loop system under the proposed control scheme is also robust to the uncertainties in CCLs and does not need to reset the local controllers.

4.7. Robustness to different subsequent changes

The objective of this case study is to examine the robustness of the proposed controller against several consecutive changes caused by different sources of uncertainty. Therefore, first DG 5 is plugged out from the test DC system at $t = 1s$ and then, an unknown resistive load is parallelly connected to the load at PCC 6 at $t = 1.4s$. Fig. 13 displays the PCC voltages of DGs 1 and 6 due to these variations. The outcomes illustrate that, 1) after a short transient, the load voltages at PCCs remain unaltered irrespective of the loads dynamics and the designed controller is robust, and 2) after PnP operation of DGs and disconnection of some distribution lines, the designed control system is still robust under the load variations, which is due to the satisfaction of all control objectives simultaneously.

4.8. Comparison to droop-based control method

In this scenario, the performance of the presented control approach is compared to a droop-based control manner proposed in [33], which comprises of the current PI control loop, voltage PI control loop, droop controller, and a secondary controller to correct the steady-state voltage

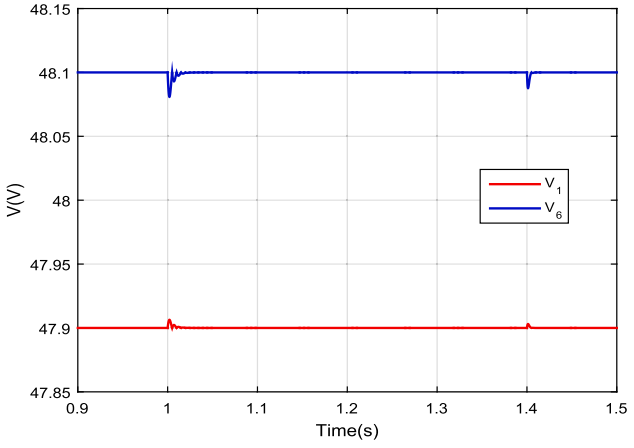

Fig. 13. PCC voltage signals of DG 1 and DG 6 due to plugging out of DG 5 and connection of an unknown load to PCC 6.

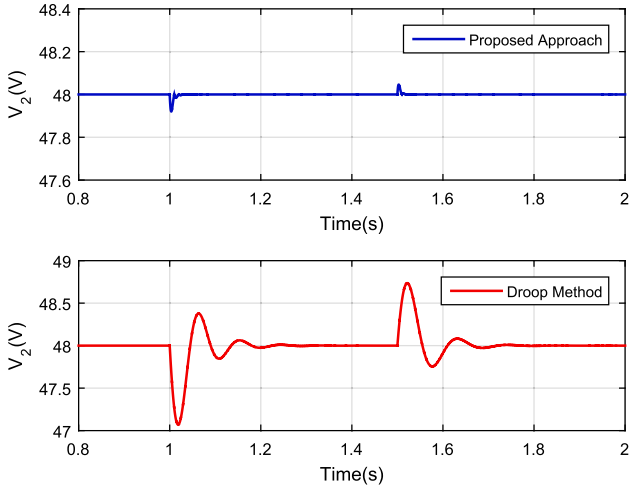

Fig. 14. Voltage signal at PCC 2 with the proposed control approach and droop-based control method in [33].

error. The performance of the closed-loop test microgrid system with the proposed control scheme and the droop-based controller against local load changes are verified. To this end, the resistance of CIL of DG 2 is stepped down from 6Ω to 3Ω at $t = 1s$, then the power of CPL of DG 2 is altered from $350W$ to $400W$ at $t = 1.5s$. Fig. 14 shows the dynamic PCC voltage of DG 2 with droop control method and the proposed decentralized control scheme due to these changes. According to the attained results, although the closed-loop test system remains stable for both control manners, the transient response of the closed-loop microgrid under the proposed robust controller is significantly improved compared to the PI-based droop controller. This is due to considering the load dynamics in the microgrid mathematical modeling in (1)–(15) and control design process, applying an effective manner to disable interaction terms between DG units, optimal design of the proposed decentralized controller, and robust desirable performance satisfaction of the closed-loop DC islanded microgrid.

5. Conclusion

A novel primary robust voltage control approach for the autonomous operation mode of DC microgrids is propounded in this paper. The microgrid system comprises of multiple DGs with arbitrary structure, and each DG has a local uncertain ZIP load. The structure of the presented primary control manner is fully decentralized and is based on the output-feedback. The proposed 2DOF controller provides robust stability for the closed-loop microgrid system. Moreover, it preserves the desirable performance of the overall system under different sources of uncertainty, including PnP functionalities of DGs, topological changes, uncertain ZIP loads, unknown load dynamics, and different subsequent changes. Every local controller is the optimal solution of a single convex optimization problem, resulting in optimal performance as well as robustness to several successive changes. Moreover, the control design procedure is scalable, i.e. the local control design for each DG is not dependent on the other DG units. All control objectives are converted into a fixed-order dynamic output feedback controller for a polytopic LTI system with H_∞ performance criterion and are formulated as an LMI-based optimization problem. The performance of the proposed controller is examined under various case studies, including reference tracking, PnP functionalities of DGs, microgrid topological variations, ZIP load changes, several subsequent changes, and comparison to the conventional droop-based method. All simulation test cases indicate that the proposed control scheme is strongly robust and retains stability and desirable performance of the closed-loop system.

As a shortcoming of the proposed control method is the disregard for the dynamics of input energy sources. To improve the performance of the provided control strategy, the following subjects are suggested for future works: 1) attaining the proposed LTI polytopic state-space model for the other types of DC/DC converters, 2) considering the dynamics of renewable energy sources in the provided mathematical model, and 3) considering other possible uncertainty sources, e.g., uncertainty in renewable energy source, in the presented polytopic model.

CRediT authorship contribution statement

Marjan Shafiee-Rad: Conceptualization, Methodology, Software, Validation, Investigation, Data curation, Writing - original draft, Visualization. **Mahdieh S. Sadabadi:** Conceptualization, Methodology, Data curation, Writing - review & editing, Visualization. **Qobad Shafiee:** Writing - review & editing, Project administration. **Mohammad Reza Jahed-Motlagh:** Supervision.

Declaration of Competing Interest

The authors declare that they have no known competing financial interests or personal relationships that could have appeared to influence the work reported in this paper.

Appendix A. Proof of Theorem 1

Proof. We must show that the condition (44) results in the stability and the H_∞ performance of the LTI system (A, B, C, D). By using the Congruence Transformation [34] and multiplying the inequality (44) from the right and left by matrix

$$\begin{bmatrix} W & 0 & 0 & 0 \\ 0 & Q & 0 & 0 \\ 0 & 0 & I & 0 \\ 0 & 0 & 0 & I \end{bmatrix} < 0,\ Q = P^{-1},\ W = M^{-1} \tag{A.1}$$

and its transposed, respectively, and then applying the Schur Complement Lemma [34], the following equivalent inequality is obtained

$$\begin{bmatrix} -(W + W^T) + \beta Q & W^T + AQ & B & 0 \\ W + QA^T & -\beta Q & 0 & QC^T \\ B^T & 0 & -\gamma I & D^T \\ 0 & CQ & D & -\gamma I \end{bmatrix} < 0. \tag{A.2}$$

According to the Schur Complement Lemma, (A.2) is equivalent to

$$\begin{bmatrix} -(W+W^T)+\beta Q & W^T+AQ & B \\ W+QA^T & \frac{1}{\gamma}QC^TCQ-\beta Q & 0 \\ B^T & 0 & \frac{1}{\gamma}D^TD-\gamma I \end{bmatrix} < 0. \tag{A.3}$$

Adding the left side of inequality (A.3) with the following negative-semidefinite matrix

$$\begin{bmatrix} 0 & 0 & \frac{1}{\gamma}QC^TD \\ 0 & 0 & -\frac{1}{\gamma}QC^TD \\ \frac{1}{\gamma}D^TCQ & -\frac{1}{\gamma}QC^TD & 0 \end{bmatrix} < 0 \tag{A.4}$$

results in the following inequality

$$\begin{bmatrix} -(W+W^T)+\beta Q & W^T+AQ & B+\frac{1}{\gamma}QC^TD \\ W+QA^T & \frac{1}{\gamma}QC^TCQ-\beta Q & 0 \\ B^T+\frac{1}{\gamma}D^TCQ & 0 & \frac{1}{\gamma}D^TD-\gamma I \end{bmatrix} < 0. \tag{A.5}$$

Again, applying the Schur Complement Lemma and using the change of variable $X=\beta Q-\frac{1}{\gamma}QC^TCQ>0$, results in the following equivalent inequality

$$\begin{bmatrix} -(W+W^T)+X & W^T+AQ & B & QC^T \\ W+QA^T & -X & 0 & 0 \\ B^T & 0 & -\gamma I & D^T \\ CQ & 0 & D & -\gamma I \end{bmatrix} < 0. \tag{A.6}$$

According to the Schur Complement Lemma, (A.6) is equivalent to

$$\begin{bmatrix} -[B \;\; QC^T]\begin{bmatrix} -\gamma I & D^T \\ D & -\gamma I \end{bmatrix}^{-1}\begin{bmatrix} B^T \\ CQ \end{bmatrix}+X-(W+W^T) & W^T+AQ \\ W+QA^T & -X \end{bmatrix} < 0, \begin{bmatrix} -\gamma I & D^T \\ D & -\gamma I \end{bmatrix} < 0. \tag{A.7}$$

Pursuant to the Reciprocal Projection Lemma [35], the feasibility of the inequality (A.7) with respect to W, in which X is any given positive-definite matrix, is equivalent to the following LMIs

$$QA^T+AQ-[B \;\; QC^T]\begin{bmatrix} -\gamma I & D^T \\ D & -\gamma I \end{bmatrix}^{-1}\begin{bmatrix} B^T \\ CQ \end{bmatrix} < 0, \begin{bmatrix} -\gamma I & D^T \\ D & -\gamma I \end{bmatrix} < 0. \tag{A.8}$$

After multiplying the right and left sides of (A.8) by matrix P, the following equivalent conditions are attained

$$A^TP+PA-[PB \;\; C^T]\begin{bmatrix} -\gamma I & D^T \\ D & -\gamma I \end{bmatrix}^{-1}\begin{bmatrix} B^TP \\ C \end{bmatrix} < 0, \begin{bmatrix} -\gamma I & D^T \\ D & -\gamma I \end{bmatrix} < 0. \tag{A.9}$$

According to the Schur Complement Lemma, (A.9) is equivalent to

$$\begin{bmatrix} A^TP+PA & PB & C^T \\ B^TP^T & -\gamma I & D^T \\ C & D & -\gamma I \end{bmatrix} < 0. \tag{A.10}$$

Based on the Bounded Real Lemma (BRL) [36], the matrix inequality (A.10) demonstrates that the linear system (A, B, C, D) is stable, and $\|C(SI-A)^{-1}B+D\|_\infty<\gamma$. □

Appendix B. Proof of Theorem 2

Proof. It should be shown that the conditions in (45) guarantee the robust stability and the robust H_∞ performance of the closed-loop system (43). The convex combination of the inequalities given in (45) brings about the following condition

$$\begin{bmatrix} -(M+M^T) & P(\theta)+M^TA_{cl}(\theta) & M^TB_{cl}(\theta) & 0 & M^T \\ * & -\beta P(\theta) & 0 & C_{cl}^T(\theta) & 0 \\ * & * & -\gamma I & D_{cl}^T(\theta) & 0 \\ * & * & * & -\gamma I & 0 \\ * & * & * & * & -\beta^{-1}P(\theta) \end{bmatrix} < 0 \tag{B.1}$$

where the matrices $(A_{cl}(\theta), B_{cl}(\theta), C_{cl}(\theta), D_{cl}(\theta))$ are given in (42), and $P(\theta)=\sum_{j=1}^{q}\theta_jP^j$.

According to Theorem 1, inequality (B.1) demonstrates that the closed-loop system $T_{wz}(\theta)$ is stable, and also $\|T_{wz}(\theta)\|_\infty<\gamma$. □

References

[1] Guerrero JM, Chandorkar M, Lee T, Loh PC. Advanced control architecture for intelligent microgrids–Part I: Decentralized and hierarchical control. IEEE Trans Ind Electron 2013;60(4):1254–62.
[2] Shafiee Q, Dragicevic T, Vasquez JC, Guerrero JM. Hierarchical control for multiple DC-microgrids clusters. IEEE Trans Energy Convers 2014;29(4):1018–31.
[3] Elsayed AT, Mohamed AA, Mohammed OA. DC microgrids and distribution systems: An overview. Electric Power Syst Res 2015;119:407–17.
[4] Lu X, Guerrero M, Sun K, Vasquez JC. An improved droop control method for DC microgrids based on low bandwidth communication with DC bus voltage restoration and enhanced current sharing accuracy. IEEE Trans Power Electron 2014;29(4):1800–12.
[5] Shafiee Q, Dragicevic T, Andrade F, Vasquez JC, Guerrero JM. Distributed consensus-based control of multiple DC-microgrids clusters. In: IECON 2014 - 40th Annu. Conf. IEEE Ind. Electron. Soc, Dallas, TX, USA, Oct.-Nov. 2014, p. 2056–62.
[6] Nasirian V, Davoudi A, Lewis FL. Distributed adaptive droop control for DC microgrids. IEEE Trans Energy Convers 2014;29(4):1147–52.
[7] Meng L, Dragicevic T, Vasquez J, Guerrero J, Sanseverino ER. Hierarchical control with virtual resistance optimization for efficiency enhancement and state-of-charge balancing in DC microgrids. IEEE 1st Int. Conf. Direct Curr. Microgrids (ICDCM), Atlanta, Georgia. 2015.
[8] Moayedi S, Davoudi A. Distributed tertiary control of DC microgrid clusters. IEEE Trans Power Electron 2016;31(2):1717–33.
[9] Xia Y, Yu M, Yang P, Peng Y, Wei W. Generation-storage coordination for islanded DC microgrids dominated by PV generators. IEEE Trans Energy Convers 2019;34(1):130–8.
[10] Hamzeh M, Emamian S, Karimi H, Mahseredjian J. Robust control of an islanded microgrid under unbalanced and nonlinear load conditions. IEEE J Emerg Sel Topics Power Electron 2016;4(2):512–20.
[11] Babazadeh M, Nobakhti A. Robust decomposition and structured control of an islanded multi-DG microgrid. IEEE Trans Smart Grid 2019;10(3).
[12] Riverso S, Sarzo F, Ferrari-Trecate G. Plug-and-play voltage and frequency control of islanded microgrids with meshed topology. IEEE Trans Smart Grid 2015;6(3):1176–84.
[13] Sadabadi MS, Shafiee Q, Karimi A. Plug-and-play voltage stabilization in inverter-interfaced microgrids via a robust control strategy. IEEE Trans. Contr. Syst. Technol. 2017;25(3):781–91.
[14] Baghaee HR, Mirsalim M, Gharehpetian G, Talebi HA. A decentralized robust mixed H2-H∞ voltage control scheme to improve small/large-signal stability and FRT capility of islanded multi-DER microgrids considering load disturbances. IEEE Syst J 2018;12(3):2610–21.
[15] Shafiee-Rad M, Shafiee Q, Jahed-Motlagh MR. Decentralized scalable robust voltage control for islanded AC microgrids with general topology. 11th IEEE Power Electronics, Drive Systems, and Technologies Conf. (PEDSTC), Tehran, Iran. 2020. p. 1–6.
[16] Cavraro G, Carli R. Local and distributed voltage control algorithms in distribution network. IEEE Trans Power Syst 2018;33(2):1420–30.
[17] Hua H, Cao J, Yang G, Ren G. Voltage control for uncertain stochastic nonlinear system with application to energy Internet: Non-fragile robust H ∞ approach. J Mathem Anal Appl 2018;463(1):93–110.
[18] Mehdi M, Saad M, Jamali SZ, Kim C. Output-feedback based robust controller for uncertain DC islanded microgrid. Trans Inst Measure Control 2020;42(6):1239–51.
[19] Mehdi M, Jamali SZ, Khan MO, Baloch S, Kim C-H. Robust control of a DC microgrid under parametric uncertainty and disturbances. Electr Power Syst Res 2020;179.
[20] Ornelas-Tellez F, Rico-Melgoza JJ, Espinosa-Juarez E, Sanchez EN. Optimal and robust control in DC microgrids. IEEE Trans Smart Grid 2018;9(6):5543–53.
[21] Amiri H, Markadeh GA, Dehkordi NM. Voltage control in a DC islanded microgrid based on nonlinear disturbance observer with CPLs. J Storage Mater 2020;29:101296.
[22] Sadabadi MS, Shafiee Q. Scalable robust voltage control of DC microgrids with uncertain constant power loads. IEEE Trans Power Syst 2020;35(1):508–15.
[23] Tucci M, Riverso S, Vasquez JC, Guerrero JM, Ferrari -Trecate G. A decentralized scalable approach to voltage control of DC islanded microgrids. IEEE Trans Control Syst Technol 2016;24(6):1965–79.
[24] Sadabadi MS, Shafiee Q, Karimi A. Plug-and-play robust voltage control of DC microgrids. IEEE Trans Smart Grid 2018;9(6):6886–96.
[25] Su M, Liu Z, Sun Y, Han H, Hou X. Stability analysis and stabilization methods of DC microgrid with multiple parallel-connected DC-DC converters loaded by CPLs. IEEE Trans Smart Grid 2018;9(1):132–42.
[26] Zhou K, Doyle JC. Essentials of robust control. Upper Saddle River, NJ: Prentice-Hall; 1998.
[27] Liu K-Z, Yao Y. Relation between time domain and frequency domain properties. Robust control theory and applications. Wiley; 2016. (ch. 8).
[28] Venkatasubramanian V, Schattler H, Zaborszky J. Fast time-varying phasor analysis in the balanced three-phase large electric power system. IEEE Trans. Automat. Control 1995;40(11):1975–82.
[29] Skogestad S, Postlethwaite I. Multivariable feedback control: analysis and design. Hoboken, NJ: Wiley; 2001.
[30] Gumussoy S, Henrion D, Millstone M, Overton ML. Multiobjective robust control with HIFOO 2.0. In: Proc. IFAC Symp. Robust Control Design, Haifa, Israel, June 2009, p. 144–49.
[31] Löfberg J. YALMIP: A toolbox for modeling and optimization in MATLAB. In: Proc. IEEE Int. Symp. Comp. Cont. Syst. Design (CACSD), 2004. [Online]. Available: http://control.ee.ethz.ch/~joloef/yalmip.php.
[32] IEEE recommended practice for monitoring electric power quality, IEEE standard 1159, 2019.
[33] Ghanbari N, Bhattacharya S, Constant power load challenges in droop controlled DC microgrids. In: IECON 2019 - 45th Annu. Conf. IEEE Ind. Electron. Soc., Lisbon, Portugal, Portugal, vol. 1, Oct. 2019, p. 3871–76.
[34] VanAntwerp JG, Bratz RD. A tutorial on linear and bilinear matrix inequalities. J Process Control 2000;10:363–85.
[35] Apkarian P, Tuan H, Bernussou J. Continuous-time analysis, eigenstructure assignment, and H2 synthesis with enhanced linear matrix inequalities (LMI) characterizations. IEEE Trans Automat Control 2001;46(12):1941–6.
[36] Boyd S, El Ghaoui L, Feron E, Balakrishnan V. Linear matrix inequality in system and control theory. Philadelphia: SIAM; 1994.